International Journal of Mechanical, Industrial and Aerospace Sciences
ISSN: 2517-9950
Vol:11, No:2, 2017

Active Control of Multiferroic Composite Shells Using 1-3 Piezoelectric Composites

S. C. Kattimani

Abstract**—**This article deals with the analysis of active constrained layer damping (ACLD) of smart multiferroic or magneto-electro-elastic doubly curved shells. The kinematics of deformations of the multiferroic doubly curved shell is described by a layer-wise shear deformation theory. A three-dimensional finite element model of multiferroic shells has been developed taking into account the electro-elastic and magneto-elastic couplings. A simple velocity feedback control law is employed to incorporate the active damping. Influence of layer stacking sequence and boundary conditions on the response of the multiferroic doubly curved shell has been studied. In addition, for the different orientation of the fibers of the constraining layer, the performance of the ACLD treatment has been studied.

Keywords**—**Active constrained layer damping, doubly curved shells, magneto-electro-elastic, multiferroic composite, smart structures.

I. Introduction

STRUCTURES integrated with piezoelectric sensors and actuators possess self-sensing, self-monitoring, and diagnosing capabilities are commonly known as smart structures. It is evident from the open literature that the piezoelectric materials are the best smart materials for the active control of high-performance light weight flexible structures [1]-[4]. In order to achieve better performance from the piezoelectric materials of low control authority, they are being used as the constraining layer of the ACLD treatment rather than directly bonded to the substrates. Furthermore, the ACLD treatment can also be used as passive constrained layer damping (PCLD) by deactivating the applied control voltages [5]. Thus, the ACLD treatment has been established as an efficient smartness element providing both passive and active damping simultaneously when under operation [6]-[10].

A unique and interesting class of multiphase composites such as multiferroic or magnetoelectroelastic (MEE) composite consisting of ferroelectric/piezoelectric (**$BaTiO_3$**) and ferromagnetic/ piezomagnetic (**$CoFe_2O_4$**) phases has attracted the interest of researchers over the last few years on account of promising properties of multiferroic composite materials. Multiphase composite structures made of ferroelectric and ferromagnetic layers are subjected to the actions of electro-elastic, magneto-elastic, and electro-magnetic coupled fields, which are absent in the individual constituents. The unique property of MEE materials is that they have the ability to covert energy among magnetic, electric and mechanical energies [11]-[16]. These interesting properties attracted the researchers to use the multiferroic materials in the fields of sensors, actuators, transducers, space structures, sonar applications. Most recently, Xin and Hu [17] studied the free vibration of simply supported multilayered MEE plates using the discrete singular convolution algorithm and state space approach. Gou et al. [18] investigated the static deformation of anisotropic four layered MEE plates under surface loading based on the modified couple-stress theory. Liu et al. [19] determined the high order solutions for MEE plates with non-uniform materials. Zhou and Zhu [20] used the third order shear deformation theory to study the vibration and bending analysis of multiferroic plates. Further, nonlinear analysis of MEE plates has attracted the interest of researchers considerably. Chen and Yu [21] developed the geometrically nonlinear multiphysics plate model and analyzed the MEE laminated composites by applying the variational asymptotic method. Shooshtari and Razavi [22] used thin plate theory to investigate a nonlinear free and forced vibration of transversely isotropic rectangular MEE thin plate. Farajpour et al. [23] investigated the nonlinear free vibration of size dependent MEE nanoplates subjected to external electric and magnetic potentials by considering the geometrical nonlinearity.

Since the MEE shell can be a promising smart composite structure and is composed of smart materials, the necessity of using the additional means of smart damping such as the ACLD treatment for the active control of the multiferroic/MEE shell must be investigated. However, to the authors' best knowledge, the research concerning the control of multiferroic shell is not yet reported. In this paper, three-dimensional analysis of the ACLD of the multiferroic doubly curved shells integrated with the patches of the ACLD treatment has been carried out by the finite element method to investigate the active control vibrations. The effects of various parameters such as the effect of coupling coefficients, boundary conditions, aspect ratio and the variation of the piezoelectric fiber orientation angle in the 1-3 PZC constraining layer on the response of the multiferroic doubly curved shells have been thoroughly investigated.

II. Problem Description

A schematic diagram of a multiferroic doubly curved shell with the ACLD patch at the center of the top surface of the shell is illustrated in Fig. 1 [5]. It may be noted that the results are also obtained by placing two patches of same volume at the edges of the top surface of the shell. The middle layer of the multiferroic shell is made of ferromagnetic

S. C. Kattimani is with the National Institute of Technology Karnataka, Surathkal-575025, India (phone: +91 824 2473661; +91 9481413661; e-mail: sck@ nitk.ac.in).

(magnetostrictive) whereas the bottom and top layers of the shell are made of ferroelectric (piezoelectric). The viscoelastic layer is sandwiched between the piezoelectric layer of the ACLD treatment and the multiferroic substrate shell. Fig. 1 (b) illustrates the vertically reinforced 1-3 PZC layer in which the piezoelectric fibers are aligned and coplanar with the **xz** plane, while their orientation angle with the **z**-axis is **λ**. The curvilinear length, the curvilinear width, and the total thickness of the MEE shell are *a*, *b* and *H*, respectively. Radii of curvature of the middle surface are assumed to be R_1 and R_2. The thickness of the constraining PZC layer and the constrained viscoelastic layer of the ACLD treatment are h_p and h_v, respectively. The material properties used in the present analysis are given in Table I [16].

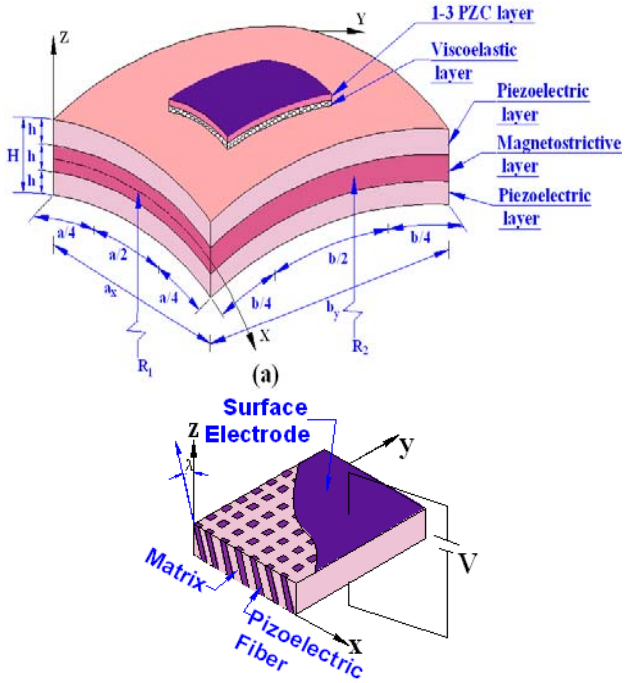

Fig. 1 (a) Schematic diagram of a P/M/P multiferroic shell integrated with a patch of ACLD treatment at the center of the shell. (b) Vertically reinforced 1-3 PZC composites

It should be noted that the density of both the material ferroelectric and ferromagnetic are used identical as given in literature [16].

A. Kinematics of Doubly Curved Shell

The rotations of transverse normal lying in the substrate are represented by $\boldsymbol{\theta}_x$ and $\boldsymbol{\theta}_y$ in the ***xz***-plane and in the ***yz***-plane, respectively. Thus, the axial displacements ***u*** and ***v*** of any point in the overall shell/plate along the ***x***- and the ***y***-directions, respectively, can be written as:

$$u(x,y,z,t) = u_0(x,y,t) + \theta_x(x,y,t)$$

$$v(x,y,z,t) = v_0(x,y,t) + \theta_y(x,y,t) \quad (1)$$

The transverse displacement assumed for the MEE shells/plates can be represented by:

$$w(x,y,z,t) = w_0(x,y,t) + z\,\theta_z(x,y,t) + z^2\,\phi_z(x,y,t) \quad (2)$$

In (1) and (2), $\boldsymbol{u}_0, \boldsymbol{v}_0$ and $\boldsymbol{w}_0$ are the translational displacements at any point on the mid-plane of the substrate along ***x***-, ***y***- and ***z***-directions, respectively, whereas, θ_z and ϕ_z are the generalized rotational displacements. To facilitate the computation and evaluation, the rotational variables $\{d_r\}$ are separated from the translational displacement variables $\{d_t\}$ and are given by:

$$\{d_t\} = \begin{bmatrix} u_0 & v_0 & w_0 \end{bmatrix}^T$$

and

$$\{d_r\} = \begin{bmatrix} \theta_x & \theta_y & \theta_z & \phi_z \end{bmatrix}^T \quad (3)$$

The states of strain and stress at any point in the overall doubly curved shell are expressed by the strain/stress vector containing in-plane strain/stress and transverse normal strain/stress and the vector of transverse shear strains/stresses can be expressed as in (4a) and (4b):

$$\{\varepsilon_b\} = \begin{Bmatrix} \varepsilon_x & \varepsilon_y & \varepsilon_z & \varepsilon_{xy} \end{Bmatrix} \text{ and } \{\varepsilon_s\} = \begin{Bmatrix} \varepsilon_{xz} & \varepsilon_{yz} \end{Bmatrix} \quad (4a)$$

$$\{\sigma_b\} = \begin{bmatrix} \sigma_x & \sigma_y & \sigma_z & \sigma_{xy} \end{bmatrix}^T \text{ and } \{\sigma_s\} = \begin{bmatrix} \sigma_{xz} & \sigma_{yz} \end{bmatrix}^T \quad (4b)$$

Making use of linear strain-displacement relations and the displacement fields, the strain vectors defining the state of in-plane and transverse normal strains and the transverse shear strains at any point in the substrate, the viscoelastic layer and the piezoelectric actuator layer, respectively, can be expressed as:

$$\{\varepsilon_b^s\} = \{\varepsilon_{bt}\} + [z_1]\{\varepsilon_{rb}\},\ \{\varepsilon_b^p\} = \{\varepsilon_{bt}\} + [z_2]\{\varepsilon_{rb}\},$$
$$\{\varepsilon_s^s\} = \{\varepsilon_{ts}\} + [z_3]\{\varepsilon_{rs}\},\ \{\varepsilon_s^v\} = \{\varepsilon_{ts}\} + [z_4]\{\varepsilon_{rs}\} \quad (5)$$

$$\{\varepsilon_s^p\} = \{\varepsilon_{ts}\} + [z_5]\{\varepsilon_{rs}\} \quad (6)$$

The superscripts s, v and p represent the substrate, the viscoelastic layer and the piezoelectric layer, respectively. The transformation matrices $[Z_1]$-$[Z_5]$ and the strain vectors appearing in (5) and (6) have been explicitly presented in the Appendix A.

B. Constitutive Equations

The coupled constitutive relations for the MEE solid substrate are given by:

$$\left\{s_b^s\right\}=\left[\bar{C}_b^s\right]\left\{e_b^s\right\}-\left\{e_b^s\right\}E_z-\left\{q_b^s\right\}H_z \text{ and } \left\{\sigma_s^s\right\}=\left[\bar{C}_s^s\right]\left\{\varepsilon_s^s\right\} \quad (7)$$

$$D_z=\left\{e_b^s\right\}^T\left\{\varepsilon_b^s\right\}+\in_{33}^s E_z+d_{33}H_z \quad (8)$$

$$B_z=\left\{q_b^s\right\}^T\left\{\varepsilon_b^s\right\}+d_{33}E_z+\mu_{33}H_z \quad (9)$$

where, $\mathbf{D_z}$ and $\mathbf{B_z}$ are the electric displacement and the magnetic induction (i.e., magnetic flux), respectively, along the **z**-direction; $\mathbf{E_z}$ and $\mathbf{H_z}$ are the electrical field and the magnetic field, respectively, along the **z**-direction; $[\bar{C}_b^s]$ and $[\bar{C}_s^s]$ are transformed elastic constitutive matrix; $\in_{33}^s$ and μ_{33} are the dielectric constant and the magnetic permeability constant, respectively; $\{e_b^s\}$, $\{q_b^s\}$ and $\mathbf{d}_{33}$ are the piezoelectric coefficient matrix, the magnetostrictive coefficient matrix and the electromagnetic coefficient, respectively. The viscoelastic material used in the present study is assumed to be linearly viscoelastic homogeneous and isotropic. In the complex modulus approach, the shear modulus **G** and the Young's modulus **E** of the viscoelastic material are given by:

$$G=G^{'}\left(1+i\eta\right) \text{ and } E=2G\left(1+\upsilon\right) \quad (10)$$

in which $G^{'}$ is the storage modulus, υ is the Poisson's ratio, and η is the loss factor at any particular operating temperature and frequency.

C. Electric Field- Potential Relations

According to the Maxwell's electromagnetic equations, the transverse electric fields E_z^t and E_z^b, and the magnetic field H_z are related to the electric potentials ϕ^t and ϕ^b, and the magnetic potential ψ in (11).

$$\mathrm{E}_\zeta^\tau=-\frac{\partial\phi^\tau}{\partial\zeta},\ E_z^b=-\frac{\partial\phi^b}{\partial z} \text{ and } H_z=-\frac{\partial\psi}{\partial z} \quad (11)$$

in which ϕ^t and ϕ^b are the electric potential functions in the top and the bottom piezoelectric layer, respectively. It is assumed that the interfaces between the piezoelectric layer and the magnetostrictive layer are suitably grounded. Also, since the thicknesses of the layers of the substrate are very small, linear variations of the electric potential and the magnetic potential functions can be assumed across the thickness of the layers. Thus, the electric potential functions ϕ^t, ϕ^b and the magnetic potential distribution field ψ in the magnetostrictive layer can be expressed as:

$$\phi^t=\frac{z-z_b}{h}\phi_1,\ \phi^b=-\frac{z-h_2}{h}\phi_2 \text{ and } \psi=\frac{z-h_2}{h}\bar{\psi} \quad (12)$$

D. Finite Element Formulation of Shell

The overall magneto-electro-elastic shell integrated with the ACLD patches is discretized by eight noded iso-parametric quadrilateral elements. In accordance with (3), the generalized displacement vectors $\{d_{ti}\}$ and $\{d_{ri}\}$ associated with the i^{th} ($i=1,2,3,...,8$) node of the element can be written as:

$$\{d_{ti}\}=\begin{bmatrix}u_{0i} & v_{0i} & w_{0i}\end{bmatrix}^T \text{ and}$$

$$\{d_{ri}\}=\begin{bmatrix}\theta_{xi} & \theta_{yi} & \theta_{zi} & \phi_{xi} & \phi_{yi} & \phi_{zi} & \gamma_{xi} & \gamma_{yi}\end{bmatrix}^T \quad (13)$$

The generalized displacement vectors, the electric potential vector $\{\phi\}$, and the magnetic potential $\{\bar{\psi}\}$ at any point within the element can be expressed in terms of the nodal generalized displacement vectors ($\{d_t^e\}$ and $\{d_r^e\}$), the nodal electric potential vector $\{\phi^e\}$, and the nodal magnetic potential vector $\{\bar{\psi}^e\}$, respectively, in (14a):

$$\{d_t\}=[N_t]\{d_t^e\},\ \{d_r\}=[N_r]\{d_r^e\},$$

$$\{\phi\}=\begin{bmatrix}\bar{\phi}_1 & \bar{\phi}_2\end{bmatrix}^T=[N_\phi]\{\phi^e\} \text{ and } \bar{\psi}=[N_\psi]\{\bar{\psi}^e\} \quad (14a)$$

in which,

$$\{d_t^e\}=\begin{bmatrix}\{d_{t1}^e\}^T & \{d_{t2}^e\}^T & . & . & . & \{d_{t8}^e\}^T\end{bmatrix}^T,$$

$$\{d_r^e\}=\begin{bmatrix}\{d_{r1}^e\}^T & \{d_{r2}^e\}^T & . & . & . & \{d_{r8}^e\}^T\end{bmatrix}^T,$$

$$\{\phi^e\}=\begin{bmatrix}\bar{\phi}_{11} & \bar{\phi}_{21} & \bar{\phi}_{12} & \bar{\phi}_{22} & . & . & . & \bar{\phi}_{18} & \bar{\phi}_{28}\end{bmatrix}^T,$$

$$\{\bar{\psi}^e\}=\begin{bmatrix}\bar{\psi}_1 & \bar{\psi}_2 & . & . & . & \bar{\psi}_8\end{bmatrix}^T,$$

$$[N_t]=\begin{bmatrix}N_{t1} & N_{t2} & . & . & . & N_{t8}\end{bmatrix},$$

$$[N_r]=\begin{bmatrix}N_{r1} & N_{r2} & . & . & . & N_{r8}\end{bmatrix},$$

$$[N_\phi]=\begin{bmatrix}n_1 & 0 & n_2 & 0 & . & . & . & n_8 & 0\\ 0 & n_1 & 0 & n_2 & . & . & . & 0 & n_8\end{bmatrix},$$

$$[N_\psi]=\begin{bmatrix}N_{\psi 1} & N_{\psi 2} & . & . & . & N_{\psi 8}\end{bmatrix},\ N_{ti}=n_i I_t,$$

$$N_{ri}=n_i I_r. \quad (14b)$$

where $[N_t]$, $[N_r]$, $[N_\phi]$, and $[N_\psi]$ are the (3 × 24), (8 × 64), (2 × 16), and (1 × 8) shape function matrices, respectively.

The control voltage $\mathbf{V^j}$ of the constraining layer of each ACLD patch is supplied according to a simple derivative control law. Thus, the control voltage for each patch can be expressed in terms of derivatives of the global nodal degrees of freedom as given in (15):

$$V^j = -K_d^j \dot{w}_o = -K_d^j \left[U_t^j\right]\left\{\dot{X}\right\} \tag{15}$$

where $\boldsymbol{K_d^j}$ is the control gains of the $\mathbf{j^{th}}$ ACLD patch, $[\boldsymbol{U_t^j}]$ is the unit vectors. Using the first variation of the total potential energy of the typical element integrated with the ACLD treatment, the final coupled equations of motion governing the closed loop dynamics of the MEE doubly curved shell integrated with the ACLD patches is expressed in (16):

$$\left[M\right]\left\{\ddot{X}\right\}+\left[K_{tt}\right]\left\{X\right\}+\left[K_{tr}\right]\left\{X_r\right\}+\left[K_{t\phi}\right]\left\{\phi\right\}+\left[K_{t\psi}\right]\left\{\psi\right\}$$
$$+\sum_{j=1}^{q}\left\{F_{tp}^j\right\}K_d^j\left[U_t^j\right]\left\{\dot{X}\right\}=\left\{F\right\}$$

$$\left[K_{tr}\right]^T\left\{X\right\}+\left[K_{rr}\right]\left\{X_r\right\}+\left[K_{r\phi}\right]\left\{\phi\right\}+\left[K_{r\psi}\right]\left\{\psi\right\}$$
$$+\sum_{j=1}^{q}\left\{F_{rp}^j\right\}K_d^j\left[U_t^j\right]\left\{\dot{X}\right\}=0$$

$$\left[K_{t\phi}\right]^T\left\{X\right\}+\left[K_{r\phi}\right]^T\left\{X_r\right\}-\left[K_{\phi\phi}\right]\left\{\phi\right\}=0$$

$$\left[K_{t\psi}\right]^T\left\{X\right\}+\left[K_{r\psi}\right]^T\left\{X_r\right\}-\left[K_{\psi\psi}\right]\left\{\psi\right\}=0 \tag{16}$$

The final closed loop global equations of motion of the MEE shell integrated with the ACLD system can be obtained as:

$$\left[M\right]\left\{\ddot{X}\right\}+\left(\sum_{j=1}^{q}\left\{F_p^j\right\}K_d^j\left[U^j\right]\right)\left\{\dot{X}\right\}+\left[K\right]\left\{X\right\}=\left\{F\right\} \tag{17}$$

in which, the global augmented matrices are given by:

$$\left[K\right]=\left[K_1\right]-\left[K_2\right]\left[K_3\right]^{-1}\left[K_2\right]^T,$$

$$\left\{F_p^j\right\}=\left[K_2\right]\left[K_3\right]^{-1}\left\{F_{rp}^j\right\}-\left\{F_{tp}^j\right\},$$

$$\left[K_{a\psi}\right]=\left[K_{t\psi}\right]\left[K_{\psi\psi}\right]^{-1}-\left[K_2\right]\left[K_3\right]^{-1}\left[K_{r\psi}\right]\left[K_{\psi\psi}\right]^{-1},$$

$$\left[K_1\right]=\left[K_{tt}\right]+\left[K_{t\phi}\right]\left[K_{\phi\phi}\right]^{-1}\left[K_{t\phi}\right]^T+\left[K_{t\psi}\right]\left[K_{\psi\psi}\right]^{-1}\left[K_{t\psi}\right]^T$$

$$\left[K_2\right]=\left[K_{tr}\right]+\left[K_{t\phi}\right]\left[K_{\phi\phi}\right]^{-1}\left[K_{r\phi}\right]^T+\left[K_{t\psi}\right]\left[K_{\psi\psi}\right]^{-1}\left[K_{r\psi}\right]^T$$

$$\left[K_3\right]=\left[K_{rr}\right]+\left[K_{r\phi}\right]\left[K_{\phi\phi}\right]^{-1}\left[K_{r\phi}\right]^T+\left[K_{r\psi}\right]\left[K_{\psi\psi}\right]^{-1}\left[K_{r\psi}\right]^T$$

III. Results and Discussion

This section deals with the analysis of the frequency responses of the multiferroic/MEE doubly curved shell integrated with the ACLD treatment computed by the finite element model derived in the preceding section. In order to validate the results of the simply supported MEE, doubly curved shell with infinite radii of curvature ($R_1 = \infty$, $R_2 = R_1$) is considered for the comparison with the results reported by Moita et al. [16] with the identical dimensions (sides $a = b = 1$ m and the thickness $\boldsymbol{H} = 0.3$ m). Table II demonstrates the some of the lower natural frequencies of MEE shell ($R_1 = \infty$, $R_2 = R_1$) for the P/M/P and the M/P/M stacking sequences. It may be observed from this table that the present results are in good agreement with those reported in [16] for both the stacking sequences of the MEE plates. However, as expected, it is noticed that some acceptable discrepancies exist in the result. This is attributed to the consideration of transverse normal strain $\boldsymbol{\varepsilon_z}$ in the present model which is neglected in [16]. Figs. 2 and 3 illustrate the comparison of frequency response functions for the transverse displacement of the active damping of a simply supported P/M/P and M/P/M multiferroic doubly curved shell, respectively, with ($\boldsymbol{K_d} \neq 0$, active damping) and without ($\boldsymbol{K_d} = 0$, passive damping) activating the ACLD patches when located at the center of the top surface and two patches placed at the edges. Figs. 4 and 5 illustrate the corresponding control voltages. It may be observed from these figures that the active ACLD treatment appreciably improves the damping characteristics and has considerable effect on the control of the transverse displacement of the shell over the passive damping with nominal control voltage. It may also be noticed that the performance of a single patch located at the center of the shell is better than the two patches located at the edges of the multiferroic doubly curved shell. Figs. 6 and 7 depict the frequency response functions for the transverse displacement of the active damping of the clamped-clamped P/M/P and

M/P/M doubly curved shells whereas Fig. 8 depicts the corresponding control voltages. It may be observed from these figures that the trend is analogous to the simply supported multiferroic shell.

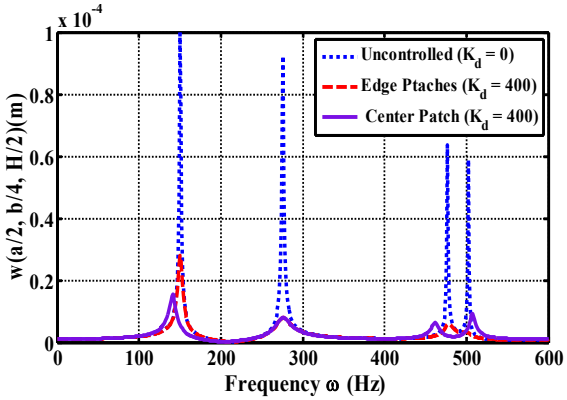

Fig. 2 Frequency response functions for the transverse displacement w(a/2, b/4, H/2) of a simply supported P/M/P multiferroic doubly curved shell (a = 200H, R_1=10a; R_2=10R_1)

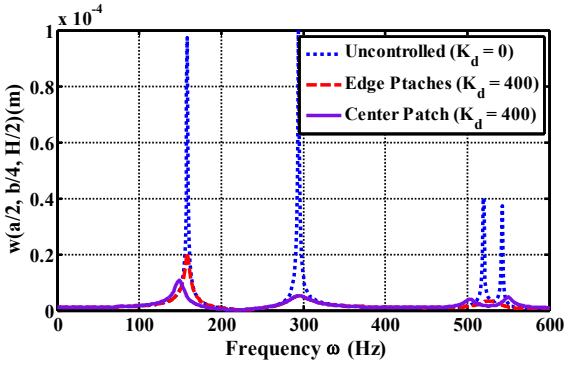

Fig. 3 Frequency response functions for the transverse displacement w(a/2, b/4, H/2) of a simply supported M/P/M multiferroic doubly curved shell (a = 200H, R_1=10a; R_2=10R_1)

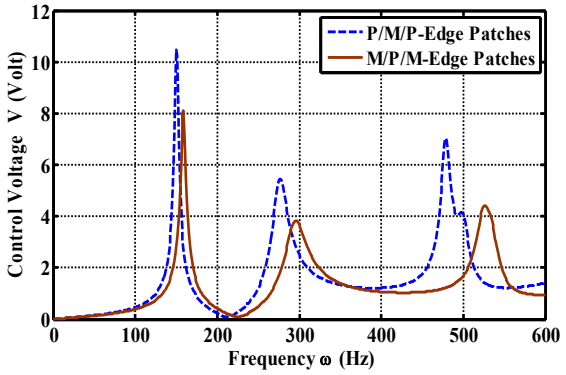

Fig. 4 Comparison of the control voltage for active damping of the simply supported multiferroic doubly curved shell when two patches placed at edges of the shell

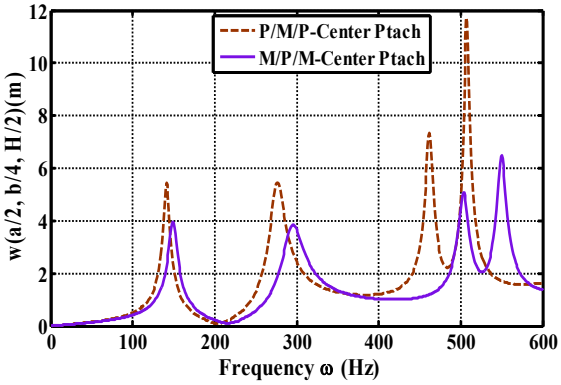

Fig. 5 Comparison of the control voltage for active damping of the simply supported multiferroic doubly curved shell when a single ACLD patch is located at center of the shell

Fig. 9 depicts the influence of piezoelectric fiber orientation angle (λ) on the responses of multiferroic shell for the P/M/P stacking sequence in the xz-plane. It is evident from this figure that the best control of amplitude of multiferroic shells is achieved by the of vertically reinforced 1-3 PZC layer (λ = 0°). It may also be noted that performance of obliquely reinforced 1-3.

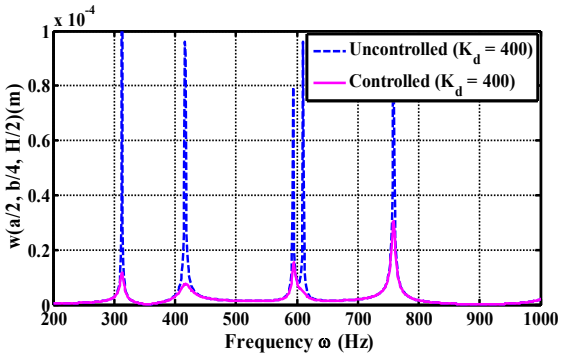

Fig. 6 Frequency response functions for the transverse displacement w(a/2, b/4, H/2) of a clamped-clamped P/M/P multiferroic doubly curved shell with patches at the edges (a = 200H, R_1=10a; R_2=10R_1)

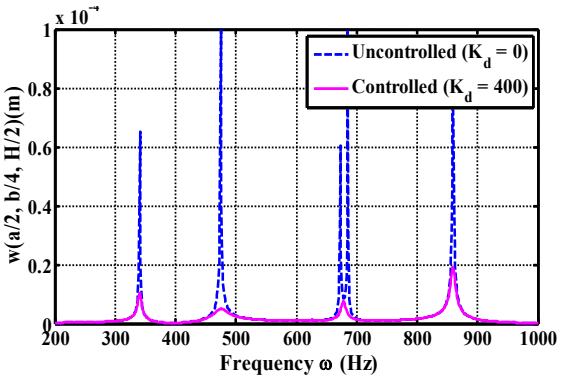

Fig. 7 Frequency response functions for the transverse displacement w(a/2, b/4, H/2) of a clamped-clamped M/P/M Multiferroic doubly curved shell with patches at the edges (a = 200H, R_1=10a; R_2=10R_1)

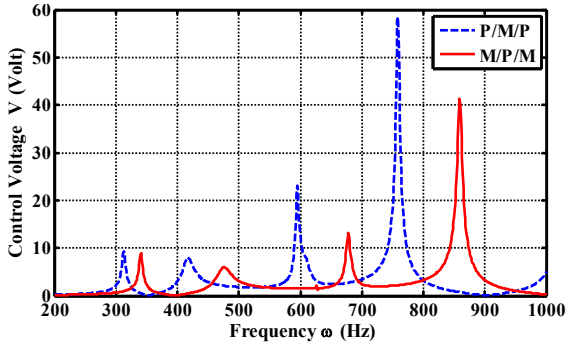

Fig. 8 Comparison of the control voltage for active damping of the clamped-clamped multiferroic doubly curved shell with patches at the edges (a = 200H, R_1=10a; R_2=10R_1)

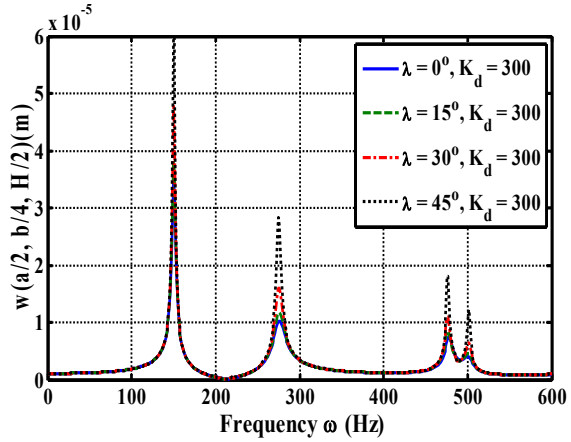

Fig. 9 Effect of variation of piezoelectric fiber orientation angle (λ) in xz-plane on the controlled response of a simply supported P/M/P multiferroic doubly curved shell (K_d = 300)

PZC constraining layer in which the piezoelectric fibers are coplanar with the **yz**-plane is better than that of the obliquely reinforced 1-3 PZC constraining layer wherein the piezoelectric fibers are coplanar with the **xz**-plane. However, for the sake of brevity, the results are not presented here. It is interesting to know that if the matrices $[K_{t\phi}]$, $[K_{\phi\phi}]$, $[K_{t\psi}]$ and $[K_{\psi\psi}]$ are set to null matrices, the responses of the multiferroic shell will be free of the effects of the electro-elastic and magneto-elastic couplings. Table III demonstrates the same in numerical values for the first three natural frequencies. It may be observed from Table III that the electro-elastic and the magneto-elastic couplings cause marginal increase in the stiffening of the P/M/P multiferroic shell. In case of the multiferroic shell controlled by the ACLD patches, the attenuation of the fundamental mode of vibration in the presence of such couplings is more than that without the presence of these couplings.

IV. Conclusions

In this paper, a three-dimensional finite element analysis has been carried out to investigate the active damping of the multiferroic doubly curved shells integrated with the patches of the ACLD treatment. The numerical results reveal that the ACLD patches significantly improve the damping characteristics of the multiferroic composite shell. The performance of the ACLD patches is influenced by the edge boundary conditions and the variation of fiber orientation angle (**λ**). The best performance of the patches is achieved when the orientation angle (**λ**) of the fibers is 0° for both simply supported and clamped-clamped multiferroic composite shell. Further, performance of single ACLD patch/treatment is better when placed at the center of the multiferroic shell than the two patches of same volume placed at the edges. The electro-elastic and magneto-elastic couplings cause marginal increase in stiffening of the multiferroic shell. These couplings improve the performance of the ACLD patches for attenuating the fundamental mode of vibration of the multiferroic shell.

APPENDIX

A. Transformation Matrices

The transformation matrices $[z_1]$, $[z_2]$, $[z_3]$, $[z_4]$ and $[z_5]$ appearing in (5) and (6) are given by:

$$[Z_1]=\left[\bar{Z}_1 \quad \ddot{O} \quad \bar{O}\right],\ [Z_2]=\left[\bar{Z}_2 \quad h_v\hat{I}_2 \quad (z-\frac{h}{2}-h_v)\hat{I}_2\right],$$

$$[Z_3]=\left[\bar{I} \quad \tilde{O} \quad \tilde{O} \quad \bar{Z}_3\right],\ [Z_4]=\left[\tilde{O} \quad \bar{I} \quad \tilde{O} \quad \bar{Z}_4\right],$$

$$[Z_5]=\left[\tilde{O} \quad \tilde{O} \quad \bar{I} \quad \bar{Z}_5\right]$$

where,

$$\bar{Z}_1=\begin{bmatrix} z & 0 & 0 & 0 & 0 \\ 0 & z & 0 & 0 & 0 \\ 0 & 0 & 0 & 1 & 2z \\ 0 & 0 & z & 0 & 0 \end{bmatrix},\ \bar{Z}_2=\frac{h}{2}\begin{bmatrix} 1 & 0 & 0 & 0 & 0 \\ 0 & 1 & 0 & 0 & 0 \\ 0 & 0 & 0 & \frac{2}{h} & \frac{4}{h}z \\ 0 & 0 & 1 & 0 & 0 \end{bmatrix},$$

$$\bar{Z}_3=\begin{bmatrix} z & 0 & z^2 & 0 \\ 0 & z & 0 & z^2 \end{bmatrix},\ \bar{Z}_4=\bar{Z}_5=\bar{Z}_3$$

B. Strain Vectors

$$\{\varepsilon_{bt}\}=\left[\frac{\partial u_0}{\partial x}+\frac{w}{R_1} \quad \frac{\partial v_0}{\partial y}+\frac{w}{R_2} \quad \frac{\partial u_0}{\partial y}+\frac{\partial v_0}{\partial x} \quad 0\right]^T,$$

$$\{\varepsilon_{ts}\}=\left[\frac{\partial w_0}{\partial x}-\frac{u_0}{R_1} \quad \frac{\partial w_0}{\partial y}-\frac{v_0}{R_2}\right]^T,$$

$$\{\varepsilon_{rs}\}=\left[\theta_x \quad \theta_y \quad \phi_x \quad \phi_y \quad \gamma_x \quad \gamma_y \quad \frac{\partial\theta_z}{\partial x} \quad \frac{\partial\theta_z}{\partial y} \quad \frac{\partial\phi_z}{\partial x} \quad \frac{\partial\phi_z}{\partial y}\right]$$

$$\{\varepsilon_{rb}\} = \left[\frac{\partial \theta_x}{\partial x} \quad \frac{\partial \theta_y}{\partial y} \quad \frac{\partial \theta_x}{\partial y} + \frac{\partial \theta_y}{\partial x} \quad \theta_z \quad \phi_z \quad \frac{\partial \phi_x}{\partial x} \frac{\partial \phi_y}{\partial y} \quad \frac{\partial \phi_x}{\partial y} + \frac{\partial \phi_y}{\partial x} \quad \frac{\partial \gamma_x}{\partial x} \quad \frac{\partial \gamma_y}{\partial y} \quad \frac{\partial \gamma_x}{\partial y} + \frac{\partial \gamma_y}{\partial x} \right]^T$$

TABLE I
MATERIAL PROPERTY OF $BaTiO_3$ AND $CoFe_2O_4$ [6], [16]

	$C_{11} = C_{22}$ (10^9 N/m^2)	C_{12} (10^9 N/m^2)	$C_{13} = C_{23}$ (10^9 N/m^2)	C_{33} (10^9 N/m^2)	$C_{44} = C_{55}$ (10^9 N/m^2)	C_{66} (10^9 N/m^2)	ρ (kg/m^3)
$BaTiO_3$	166	77	78	162	43	44.5	5800
$CoFe_2O_4$	286	173	170.5	269.5	45.3	56.5	5300
	$e_{31} = e_{32}$ (C/m^2)	e_{33} (C/m^2)	$e_{24} = e_{15}$ (C/m^2)	$\in_{11}=\in_{22}$ (10^{-9} C^2/Nm^2)	$\in_{33}$ (10^{-9} C2/Nm^2)	$\mu_{11} = \mu_{22}$ (10^{-6} Ns2 /C2)	μ_{33} (10^{-6} N s^2 /C^2)
$BaTiO_3$	-4.4	18.6	11.6	11.2	12.6	5	10
	$q_{31} = q_{32}$ (N/Am)	q_{33} (N/Am)	$q_{24} = q_{15}$ (N/Am)	$\in_{11} = \in_{22}$ (10^{-9} C^2/Nm^2)	$\in_{33}$ (10^{-9} C^2/Nm^2)	$\mu_{11} = \mu_{22}$ (10^{-6} Ns^2 /C^2)	μ_{33} (10^{-6} N s^2 /C^2)
$CoFe_2O_4$	180.3	699.7	550	0.08	0.093	-590	157

TABLE II
COMPARISON OF NATURAL FREQUENCIES (RAD/S) OF MEE PLATE ($R_1 = \infty$, $R_2 = R_1$) OBTAINED IN THE PRESENT ANALYSIS WITH THE RESULT OF MOITA ET AL. [16]

	P/M/P		**M/P/M**	
Mode	Present	[16]	Present	[16]
1	12968.55	13024.78	14298.28	15043.32
2	24465.17	25401.26	25467.34	27880.80
3	26276.83	26256.34	28048.07	28795.37
4	34711.24	35206.62	38056.24	37753.16
5	38861.78	38671.99	40460.54	41649.71

TABLE III
EFFECT OF COUPLED FIELDS ON THE NATURAL FREQUENCIES OF THE **P/M/P** MULTIFERROIC SHELL ($a = 200h$, $R_1 = 10a$, $R_2 = 10R_1$)

Mode **P/M/P**	Uncoupled fields Frequency (ω)	Coupled fields Frequency (ω)
1	149.0	152.3
2	214.8	221.9
3	282.2	289.1

REFERENCES

[1] Ray, M. C., Bhattacharya, R. and Samanta, B. (1993), "Exact Solutions for Static Analysis of Intelligent Structures", *AIAA Journal*, Vol. 31, pp.1684-1691.

[2] Reddy, J. N. (1999), "On laminate composite plates with integrated sensors and actuators", *Engineering Structures*, Vol.21, No.7, pp.568–593.

[3] Baz, A. and Ro, J. (1996), "Vibration control of plates with active constrained layer damping", *Smart Materials and Structures*, Vol. 5, pp.272–280.

[4] Ray, M. C., Oh, J. and Baz, A. (2001), "Active constrained layer damping of thin cylindrical shells", *Journal of Sound and Vibration,* Vol.240, No.5, pp. 921–935.

[5] Kattimani, S.C. and Ray, M. C., (2014a), "Active control of large amplitude vibrations of smart Magneto-electro-elastic doubly curved shells", *International Journal of Mechanics and Materials in Design*, DOI 10.1007/s10999-014-9252-3.

[6] Kattimani, S.C. and Ray, M. C., (2014b), "Smart damping of geometrically nonlinear vibrations of magneto-electro-elastic plates", *Composite Structures*, Vol. 114, pp. 51-63.

[7] Kattimani S.C. and Ray M.C. (2015), "Control of geometrically nonlinear vibrations of functionally graded Magneto-electro-elastic plates", *International Journal of Mechanical Sciences*, Vol. 99, pp.154-167.

[8] Baz, A. (1998), "Robust control of active constrained layer damping", *Journal of Sound and Vibration*, Vol. 211, No.3, pp.467-480.

[9] Ray, M. C. and Mallik, N. (2004), "Active control of laminated composite beams using a piezoelectric fiber reinforced composite layer", *Smart Materials and Structures*, Vol.13, No.1, pp.146–152.

[10] Ray, M. C. and Pradhan, A. K. (2006), Performance of vertically reinforced 1–3 piezoelectric composites for active damping of smart structures", *Smart Materials and Structures*, Vol.15, No.1, pp. 631–641.

[11] Pan, E. and Heyliger, P. R. (2002), "Free vibrations of simply supported and multilayered magneto-electro-elastic plates", *Journal of Sound and Vibration*. Vol.252, No.3, pp.429-442.

[12] Ramirez, F., Heyliger, P. R. and Pan, E. (2006), "Discrete layer solution to free vibrations of functionally graded magneto-electro-elastic plates", *Mechanics of Advanced Materials and Structures*, Vol. 13, pp. 249–266.

[13] Buchanan, G. R. (2004), "Layered versus multiphase magneto-electro-elastic composites", *Composites: Part B*. Vol. 35, pp. 413-420.

[14] Garcia Lage, R., Mota Soares, C.M., Mota Soares, C. A. and Reddy, J. N. (2004), "Layerwise partial mixed finite element analysis of magneto-electro-elastic plates", *Computers & Structures*, Vol.82, pp.1293-1301.

[15] Wang, J., Lei, Q. and Feng, Q. (2010), "State vector approach of free-vibration analysis of magneto-electro-elastic hybrid laminated plates", *Composite structures*, Vol.92, pp.1318-1324.

[16] Moita, J. M. S., Mota Soares, C. M. and Mota Soares, C. A. (2009), "Analysis of magneto-electro-elastic plates using higher order finite element model", *Composite structures*, Vol.91, pp. 421-426.

[17] Xin L., Hu Z., (2015), "Free vibration of simply supported and multilayered magneto-electro-elastic plates", *Composite structures,* Vol. 121, pp. 344-350.

[18] Guo J., Chen J. and Pan E (2016), "Static deformation of anisotropic layered magnetoelectroelastic plates based on modified couple-stress theory", *Composites Part B: Engineering*, Vol. 107, pp.84-96.

[19] Liu J., Zhong P., Gao L., Wang W. and Lu S., (2016), "High order solutions for the magneto-electro-elastic plate with non-uniform materials", *International Journal of Mechanical Sciences*, Vol. 115-116, pp.532-551.

[20] Zhou Y. and Zhu J., (2016), "Vibration and bending analysis of multiferroic rectangular plates using third order shear deformation theory", *Composite Structures*, Vol. 153, pp.712-723.

[21] Chen, H. and Yu, W., (2014), "A multiphysics model for magneto-electro-elastic laminates" *European Journal of Mechanics A/Solids*, Vol.47, pp.23-44.

[22] Shooshtari A., Razavi S. (2015a), "Nonlinear vibration analysis of rectangular magneto-electro-elastic thin plates", *IJE Transactions A: Basics*, Vol. **28**, No. 1, pp. 136-144.

[23] Farajpour A., Hari Yzdi M.R., Ratgoo A., Loghmani M., Mohammadi M., (2016), "Nonlocal nonlinear plate model for large amplitude vibration of magneto-electro-elastic nanoplates", *Composite Structures*, Vol. 140, pp.323-336.